Deviance detection in physiologically identified cell types in the rat auditory cortex

David Pérez-González[1,2], Gloria G. Parras[1,2], Camilo J. Morado-Díaz[1,2], Cristian Aedo[1,2], Guillermo V. Carbajal[1,2], Manuel S. Malmierca[1,2,3*]

[1]Cognitive and Auditory Neuroscience Laboratory (Lab 1), Institute of Neuroscience of Castilla y León (INCYL), University of Salamanca, Salamanca, Spain
[2]Salamanca Institute for Biomedical Research (IBSAL), Spain
[3]Department of Cell Biology and Pathology, Faculty of Medicine, University of Salamanca, Spain

*Corresponding author: msm@usal.es

ABSTRACT

Auditory deviance detection is a function of the auditory system that allows reduction of the processing demand for repetitive stimuli while stressing unpredictable ones, which are potentially more informative. Deviance detection has been extensively studied in humans using the oddball paradigm, which evokes an event-related potential known as mismatch negativity (MMN). The same stimulation paradigms are used in animal studies that aim to elucidate the neuronal mechanisms underlying deviance detection. In order to understand the circuitry responsible for deviance detection in the auditory cortex (AC), it is necessary to determine the properties of excitatory and inhibitory neurons separately. Measuring the spike widths of neurons recorded extracellularly from the anaesthetized rat AC, we classified them as fast spiking or regular spiking units. These two neuron types are generally considered as putative inhibitory or excitatory, respectively. In response to an oddball paradigm, we found that both types of units showed similar amounts of deviance detection overall. When considering each AC field separately, we found that only in A1 fast spiking neurons showed higher deviance detection levels than regular spiking neurons, while in the rest of the fields there was no such distinction. Interpreting these responses in the context of the predictive coding framework, we found that the responses of both types of units reflect mainly prediction error signaling (i.e., genuine deviance detection) rather than repetition suppression.

Keywords: spike width, fast spiking, regular spiking, inhibitory, excitatory, predictive coding

1 Introduction

Deviance detection is the capacity of the nervous system to filter out repetitive, non-informative stimuli while stressing unpredictable ones, which may be highly relevant for the individual. In the auditory domain, deviance detection is reflected in the form of an event-related potential known as mismatch negativity (MMN), which has been mostly studied in humans. MMN is evoked using an oddball paradigm, where a sequence of repetitive sounds (standard) is randomly broken by the presentation of a different, rare sound (deviant) (Näätänen et al., 1978). Thus, MMN is the differential response to a given sound when it is presented as a deviant, compared to when it is presented as a standard. MMN is pre-attentional (it can be recorded during sleep or even anaesthesia) (Garrido et al., 2009) and has been found altered in some pathologies such as schizophrenia (Michie et al., 2016a, 2016b), Alzheimer's disease (Tsolaki et al., 2017), or autism spectrum disorders (Vlaskamp et al., 2017), so it has potential applications as a diagnostic tool (Näätänen et al., 2012), and can be used in non-cooperative patients such as those in coma.

Several animal studies have recorded the responses of auditory neurons using the same oddball paradigms as in MMN human studies, in order to understand the neuronal basis of MMN. The general agreement in those studies is that some auditory neurons may reduce their response when a sound is presented as standard, while they have a comparatively stronger response to the same sound when it is presented as deviant. This particular type of adaptation is referred to as stimulus-specific adaptation (SSA), and could be interpreted as a neuronal mechanism involved in deviance detection (for a review, see Pérez-González and Malmierca, 2014). Neurons exhibiting high levels of SSA have been found both in the auditory cortex (Nieto-Diego and Malmierca, 2016; Parras et al., 2017; Ulanovsky et al., 2003) and in subcortical nuclei (auditory midbrain: Duque et al., 2012; Malmierca et al., 2009; Pérez-González et al., 2005; and thalamus: Antunes et al., 2010; Antunes and Malmierca, 2014), being more prominent in non-lemniscal areas (Ayala et al., 2016, 2013; Ayala and Malmierca, 2013; Duque et al., 2012). The role of corticofugal projections is still under study; current evidence suggests that subcortical SSA is not inherited from the cortex, but can be modulated by corticofugal projections (Anderson and Malmierca, 2013; Ayala et al., 2015; Malmierca et al., 2015). The differential

responses to deviant and standard stimuli can be caused simply by neuronal adaptation, reducing the response to the repetitive sound, or by genuine deviance detection, where the appearance of an unexpected sound would result in an enhanced response to the deviant. In order to separate the contributions of each of these mechanisms, responses to deviant and standard stimuli can be compared to the responses to a control sequence accounting for the repetitiveness as well as the expectancy of the stimuli (Carbajal and Malmierca, 2018).

MMN and SSA responses can be best interpreted now under the perspective of the predictive coding framework, which can explain some aspects of these neural responses (Carbajal and Malmierca, 2018; Friston, 2005). According to this theory, past events are used to generate an internal model that is used to predict new events. Those events that do not match the model would generate a prediction error (analogous to the previously mentioned genuine deviance detection), which would favor the processing of the novel event and an update of the model. On the other hand, events that match the expectations of the model, such as sequences of repetitive sounds, are already represented in the model and do not require further processing effort, leading to repetition suppression (analogous to the adaptation to repetitive sounds). The predictive coding theory assumes a hierarchy of sensory processing levels, where the outputs of one level would inform the other levels in order to update the internal model.

In order to match the abstract concepts of the deviance detection framework with actual neural elements, and possibly establish a potential neural circuit for deviance detection, it would be helpful to identify which neurons contribute to each component of deviance detection, such as repetition suppression and prediction error. The strong and distinct MMN and SSA responses, as well as the connectivity, microcircuitry and neuronal organization of the auditory cortex (AC) make this region an ideal place to identify such components.

Although there is considerable variation in the organization of the AC across mammals, it is generally accepted that the AC is made of primary fields with clear tonotopic representation of the audible frequencies, surrounded by belt or secondary, high order fields (Malmierca, 2015; Winer et al., 1999). In the rat AC, the primary fields include A1, the anterior (AAF) and the ventral (VAF) fields while

the secondary fields include the posterior (PAF) and suprarhinal (SRAF) fields (Pandya et al., 2008; Polley et al., 2007; Profant et al., 2013). A1 and VAF receive inputs predominantly from lemniscal subcortical areas, while AAF, SRAF and PAF receive inputs from non-lemniscal areas (Smith et al., 2012). As in other sensory cortices, the rat AC is made of 6 layers, each with a particular set of cell types. Excitatory pyramidal neurons are mainly located in layers III and V, although some 'spiny' stellate excitatory neurons also occur in layer IV, while different types of inhibitory interneurons are found in layers I–VI (Budinger and Kanold, 2018). While these two groups of neurons are readily differentiable using histological techniques, their identification using extracellular electrophysiological recordings is not a trivial issue. However, recording from the somatosensory cortex of unanesthetized macaques, Mountcastle et al. (1969) proposed that pyramidal neurons have wide spikes, while other non-pyramidal cortical neurons (which they refer to as potential Golgi type II neurons; likely these neurons correspond to the basket neurons that are known to be inhibitory and a possesses a stellate like morphology but lack spines) have 'thin spikes'. Since then, multiple studies in different cortical areas have used similar classifications (rat: Hefti and Smith, 2000; cat AC: Atencio and Schreiner, 2008; mouse AC: Chen et al., 2015; Natan et al., 2015; rat medial prefrontal cortex: Baeg et al., 2001; rat somatosensory cortex: Andermann et al., 2004; Bruno and Simons, 2002; macaque motor cortex: Mendoza et al., 2016; human middle temporal gyrus: Peyrache et al., 2012) where regular spiking (RS) units are considered as putative excitatory neurons while fast spiking (FS) units are considered inhibitory neurons. Hence, cortical neurons can be categorized as putative excitatory and inhibitory based on the shape of their spike waveforms and their firing rates.

In the present study we recorded neurons from the AC of the anaesthetized rat and classified them as putative excitatory or inhibitory units. We aimed to test whether they have different deviance detection properties. Results show that overall, deviance detection occurs in both excitatory and inhibitory neurons.

2 Material and methods

2.1 Data collection

This study analyses the spike waveforms from a data set of 282 neuronal recordings, originally collected for other studies regarding neuronal adaptation and predictive coding in the AC. Some of these original studies are already published (Parras et al., 2019, 2017). All methodological procedures were approved by the Bioethics Committee for Animal Care of the University of Salamanca (USAL-ID-195) and performed in compliance with the standards of the European Convention ETS 123, the European Union Directive 2010/63/EU and the Spanish Royal Decree 53/2013 for the use of animals in scientific research.

2.2 Surgical procedures

The recordings were performed in 86 urethane-anesthetized female Long Evans adult rats (body weight 200-250 g). For a full description of the surgical procedures, see (Parras et al., 2017). In summary, animals were anesthetized (urethane 1.5 g/kg i.p. and 0.5 g/kg for supplementary doses when needed). Depth of anesthesia was assessed by pedal reflex. Body temperature was monitored by a probe and maintained by a thermal blanket. Normal hearing was assessed by recording the auditory brainstem response (ABR; 0.1 ms clicks, 10-90 dB). The trachea was cannulated to allow artificial ventilation, while expired [CO_2] was monitored using a capnograph. Then, the animals were placed in a stereotaxic frame, equipped with modified ear bars that allowed the placement of speakers for auditory stimulation. A craniotomy was performed to expose the left AC, and the underlying dura was removed. The exposed cortex was then covered with a layer of agar to prevent desiccation. A tungsten microelectrode was placed orthogonal to the brain surface, and advanced by means of a piezoelectric micromanipulator (Sensapex), in order to record the extracellular activity of AC single neurons. The displacement of the micromanipulator was used to measure the depth of the electrode tip relative to the brain surface.

2.3 Acoustic stimulation

Both acoustic stimuli generation and neuronal potential recordings were performed using a RZ6 Multi I/O Processor (Tucker-Davis Technologies), controlled by custom software created with MATLAB

(MathWorks) and OpenEx Suite (Tucker-Davis Technologies). Acoustic stimuli were delivered monaurally to the ear contralateral to the recording side through calibrated speakers in a close-field configuration. The output of the system had a flat spectrum at 76 dB SPL (±3 dB) between 500 Hz and 45 kHz, and the second and third harmonic components in the signal were ≤ 40 dB below the level of the fundamental at the highest output level. Stimuli consisted of 75 ms pure tones (0.5–45 kHz), including 5 ms rise/fall ramps. The presentation rate for the majority of units was 4 stimuli/s, however for some recordings it was 3/s (27%) or 2/s (13%), due to the characteristics of the original experiments. The frequency response area was measured for each neuron, presenting tones of different frequencies (0.5–45 kHz) and intensities in random order (3-5 repetitions of each frequency-intensity combination), and was used to estimate the minimum threshold (i.e., the lowest SPL able to evoke a response) and the characteristic frequency (i.e., the tone frequency able to evoke a response the minimum threshold).

After that, pure tones were presented in oddball sequences to test for the adaptation and deviance detection properties of the neuron. For that, a pair of pure tones (f_1, f_2) within the frequency response area of the neuron were chosen, ~0.5 octaves apart, both at the same sound level (10–30 dB above minimum threshold). Each oddball sequence, which included 400 stimuli, consisted of a repetitive tone (standard, 90% probability), occasionally replaced by a different tone (deviant, 10% probability), in a pseudorandom manner. The sequence always started with at least 10 standard tones, and each deviant tone was preceded by at least 3 standard tones. On a subsequent oddball sequence, the relative probabilities of f_1 and f_2 were exchanged, in order to compensate for the neuron responding differently to each sound frequency, so we could compare the responses to each frequency when it was presented as a standard with the responses to the same frequency when it was presented as a deviant. The differential response to standard and deviant tones is known as stimulus-specific adaptation (SSA), which is considered to reflect two different components: repetition suppression and deviance detection (Carbajal and Malmierca, 2018).

In order to break down both components of SSA, we used the many-standards and the cascade control sequences, which lack the stimulus repetition of the oddball sequence. Both sequences were also 400

stimuli long, and featured pure tones at the same presentation rate, duration and sound level as in the oddball sequence. In both cases 10 frequencies were used (the same in both control sequences), including those in the oddball sequence, and the separation between two consecutive frequencies was also ~0.5 octaves. In the many-standards sequence all 10 frequencies were presented randomly, with the same probability of occurrence (10% each tone), with the restriction that all tones must be presented before the next repetition. On the other hand, in the cascade sequences the tones were sorted by increasing or decreasing frequency, and the tone preceding the probe tone was always the same as in the corresponding oddball sequence.

2.4 Electrophysiological recording

Extracellular neuronal potentials were recorded using custom-made glass-coated tungsten microelectrodes (1–4MΩ impedance at 1 kHz). The signal was digitized at 25 kHz by a RA16PA Medusa preamplifier (TDT) and sent to the RZ6 for further processing and visualization. Potentials were band-pass filtered between 0.5 and 3 kHz. Initial spike discrimination was done manually setting a voltage threshold at a level that included action potential events but excluded the baseline noise, by a trained experimenter. These events were stored for further offline processing.

2.5 Analysis of spike waveforms

The first step of offline processing was spike sorting, which allowed removal of recorded artifacts and noise, and occasionally separate single units. Spike sorting was performed on OpenSorter (Tucker-Davis Technologies), using a supervised Bayesian procedure. Spike waveforms were aligned on the trough. The mean waveform of the spikes of each unit was calculated, and the following measurements were made on the average waveform: time and voltage of the peak and trough, spike amplitude (peak-to-trough) and spike half-width (spike width at 50% of the peak-to-trough amplitude; hereinafter “spike width”) (Fig. 1A). We used the peak-to-trough signal to noise ratio (SNR) as an indicator of the quality of the spikes. The SNR was calculated as the difference between the maximum and minimum voltages, divided by the standard deviation of the background noise (when there were no spikes). Only units with an SNR > 5 were included in the study (Fig. 1B). The average number of

spikes per sorted unit was 3207 ± 4765 spikes (range: 21–35610 spikes) (Fig. 1C); about 95% of the units included more than 200 spikes.

Interspike intervals were measured over the oddball sequences for each unit, and were expressed as its reciprocal, the instantaneous firing rate (Kostal et al., 2018). We then calculated the distribution of instantaneous firing rates for each unit, and took as reference for the neuronal discharge the values of the 50^{th}, 25^{th}, 10^{th}, 5^{th} and 1^{st} percentiles, in order to account for the average as well as for the fastest firing rates that each neuron could achieve, respectively.

2.6 Statistical analysis

All statistical analyses were performed in MATLAB. Since most value distributions did not hold the normality assumption (both by visual inspection and by the results of the Lilliefors normality test), non-parametric tests were employed in this study. We used the Wilcoxon rank-sum test to check whether two independent samples came from distributions with equal medians. The sign test was used to determine whether the median of a group was different from zero. When performing comparisons between two groups (or comparing one group to zero) multiple times (e.g., Fig. 4F, Fig 5), the resulting p-values were corrected using the Holm-Bonferroni method. For comparisons of distributions between more than two groups (e.g., all the comparisons between cortical fields), the Kruskal-Wallis test was used; post hoc comparisons to find differences between groups were made using the Bonferroni method. The average values of the distributions are expressed as mean ± SD unless indicated otherwise. Null hypotheses were rejected at a significance level of 0.05.

We compared the response to each test stimulus when it adopted the role of a standard (STD) or deviant (DEV) tone in an oddball sequence, and also when it was part of a control sequence (CTR). For the subsequent analyses we used the cascade sequence as control, since the responses to the many-standards sequence were very similar (Parras et al., 2017). Baseline-corrected spike count responses of a neuron to the same tone in the three conditions (DEV, STD, CTR) were normalized using the formulas:

$$DEV_{Normalized} = DEV/N$$

$$STD_{Normalized} = STD/N$$

$$CTR_{Normalized} = CTR/N$$

where

$$N = \sqrt{DEV^2 + STD^2 + CTR^2}$$

is the Euclidean norm of the vector (DEV, STD, CTR) defined by the three responses, which can take values in the range 0–1. From these normalized responses, the *indexes of Neuronal Mismatch*, *Repetition Suppression*, and *Prediction Error* were calculated in the following way:

$$Index\ of\ Neuronal\ Mismatch = DEV_{Normalized} - STD_{Normalized}$$

$$Index\ of\ Repetition\ Suppression = CTR_{Normalized} - STD_{Normalized}$$

$$Index\ of\ Prediction\ Error = DEV_{Normalized} - CTR_{Normalized}$$

These indexes always range between −1 and 1, and allow the separation of neuronal mismatch into repetition suppression and prediction error:

$$Index\ of\ Neuronal\ Mismatch = Index\ of\ Repetition\ Suppression + Index\ of\ Prediction\ Error$$

The *index of neuronal mismatch* is largely equivalent to the typical "SSA index", commonly used in previous studies of SSA in single units (Casado-Román et al., 2019; Parras et al., 2019, 2017).

The spontaneous firing rates were measured in the periods between stimuli (during the period of 50 ms before each stimulus), which were pooled for each sequence. In contrast to measuring the spontaneous activity before each sequence, this method captures better the potential activity drifts that may occur during the sequences. On the other hand, in some cases we may be overestimating the spontaneous activity, since long latency or sustained responses evoked by the previous stimulus may occasionally fall within that period, but in general this was not the case. Some examples of PSTHs of recordings such as those included in this study are shown in Parras et al. (2019, 2017).

3 Results

3.1 Fast spiking and regular spiking neurons

We performed 282 recordings from the AC of 86 urethane-anaesthetized rats (median: 2 sites per animal, range: 1–18). Using spike sorting, we were able to collect 323 well isolated single units (241, 37 and 4 sites yielded 1, 2 and 3 units per site, respectively) and measure their spike waveforms. Only units with an SNR > 5 were included in the subsequent analyses (n = 231). Figure 2A shows the distribution of spike widths in our sample. The average spike width was 0.385 ± 0.263 ms (range: 0.134 – 1.353). These units were classified as regular spiking (RS) or fast spiking (FS) depending on the shape of the spike width distribution, which has a bimodal appearance with a prominent peak towards narrow spike widths and a spread plateau towards wider spike widths. According to this distribution, we set a cut-off at 0.35 ms; units with spike widths larger than 0.35 ms were classified as RS (Fig. 2A, orange), and the rest, i.e. units with spike widths shorter than 0.35 ms, as FS (Fig. 2A, blue). In our sample, 60 (26%) units were classified as RS, and the rest as FS (n = 171, 74%). The average spike width of RS units was 0.779 ± 0.230 ms, while that of FS units was 0.247 ± 0.039 ms (Fig. 2B). In agreement with previous studies, as we describe next, units classified using this criterion also showed different firing rates.

The neuronal responses were recorded during auditory stimulation using an oddball paradigm, which consists of a sequence of repeated tones (standards), where 10% of the occurrences are replaced by a deviant tone. This type of sequence tends to produce adaptation of the firing rate during the repetitions of the standard tones and an increased firing rate whenever a deviant tone occurs. We measured the firing rates in the periods between stimuli (during the period of 50 ms before each stimulus), in order to estimate the spontaneous firing rates, but there were no differences between RS and FS units (p = 0.129, Wilcoxon rank-sum test).

To better analyse the varying firing rates during the oddball sequences, we calculated the distribution of interspike intervals for each unit, and from there we derived the distribution of instantaneous firing rates. FS units showed on average larger firing rates than RS units for the 25th, 10th ($p < 0.01$), 5th and 1st percentiles ($p < 0.001$), but not for the 50th percentile (Wilcoxon rank-sum test, Holm-Bonferroni

corrected) (Fig. 2C). This result indicates that FS units are able to achieve higher firing rates than RS units given the proper conditions. The 1st and 5th percentiles of the distribution of firing rates are better indicators of the faster firing rates that a neuron can achieve in near-optimal conditions, since other measurements such as the median (50th percentile) would include a larger proportion of spikes that occur during less-favourable conditions, e.g. when there is no stimulus present or when the neuron is under the effect of adaptation (see Supplementary Fig. 1).

3.2 Location in auditory cortex fields

Based on stereotaxic coordinates and response characteristics, we assigned 205 units to any of the five main fields of the rat AC (Fig. 3A). Thus, 111 units were located in lemniscal fields (A1, n = 66; VAF, n = 33; AAF, n = 12) and 94 in non-lemniscal fields (SRAF, n = 47; PAF, n = 47). Lemniscal fields contained a larger proportion of FS units (81% across all lemniscal fields; A1, 85%; VAF, 70%, AAF, 92%) than non-lemniscal fields (65% across all non-lemniscal fields; SRAF, 64%; PAF, 66%). When comparing the spike widths of both types of units across AC fields, we found no differences for RS units (Kruskal-Wallis, χ^2 (4, N = 54) = 4.04, p = 0.401) nor for FS units (Kruskal-Wallis, χ^2 (4, N = 151) = 8.54, p = 0.074) (Fig. 3B).

3.3 Spike amplitude

To look for differences between RS and FS units, we measured the peak-to-trough amplitude (see Fig. 1A) of the average spike waveforms. We found that RS units had larger amplitudes than FS spikes. The peak-to-trough amplitude of RS units (571.76 ± 510.59 μV) was much larger than the amplitude of FS units (147.61 ± 93.55 μV; $p < 0.001$, Wilcoxon rank-sum test) (Fig. 3C). The spike amplitudes were similar among AC fields for RS units (Kruskal-Wallis, χ^2 (4, N = 54) = 3.27, p = 0.514) and FS units (Kruskal-Wallis, χ^2 (4, N = 151) = 1.68, p = 0.514) (Fig. 3D).

Similarly, the signal-to-noise ratio (SNR) of RS units (20.2 ± 10.3) was significantly larger than the SNR of FS units (11.6 ± 5.4; $p < 0.001$, Wilcoxon rank-sum test) (Supplementary Fig. 2A). As happened in the case of the spike amplitude, there were no differences in the SNR between AC fields for RS units (Kruskal-Wallis, χ^2 (4, N = 54) = 4.05, p = 0.400) nor for FS units (Kruskal-Wallis, χ^2 (4, N = 151) = 0.31, p = 0.989) (Supplementary Fig. 2B).

3.4 Cortical layer location

In order to check whether RS and FS units had any preferential location across the cortical layers, we recorded the depth of the electrode tip from the brain surface for 202 units. The most superficially located unit was recorded at 115 μm, while the deepest unit was found at 1170 μm (mean: 584 ± 247 μm). RS and FS units were found at similar depths (596 ± 238 vs. 579 ± 251 μm, respectively; p = 0.800, Wilcoxon rank-sum test) (Fig. 4A).

In order to estimate which layers were more likely to contain RS or FS units, we calculated the density of units in each layer, in terms of units per 100 μm (based on our sample of 202 located neurons) (Fig. 4B, left). The borders between the cortical layers were based on the depths previously reported in rat by Games and Winer (1988). We found a higher density of RS units within the approximate limits of layers III–V (5.8–12 units per 100 μm), while FS units spread from layer II to layer V (14–18.9 units per 100 μm). The estimated density of FS units was larger than RS units in all layers.

We also calculated the unit density in supragranular (layers I–III) and infragranular layers (layers V–VI) (Fig. 4B, right) separately. The unit density on both sides of the granular layer was very similar for both RS units (4.2 vs 3.3 units per 100 μm, respectively) and FS units (12.4 vs 11.9 units per 100 μm, respectively).

There were no significant differences between AC fields in the depth at which RS units (Kruskal-Wallis, χ^2 (4, N = 54) = 9.30, p = 0.054) nor FS units (Kruskal-Wallis, χ^2 (4, N = 148) = 5.20, p = 0.267) were recorded (Fig 4C).

3.5 Adapting properties of fast spiking and regular spiking neurons

From the original sample, we recorded the responses of 211 neurons to an oddball paradigm and the corresponding cascade and many-standards control sequences. Previous works have established that both control sequences produce similar results (Parras et al., 2017; Wiens et al., 2019); hence, in the present study we only used the cascade control, since it has been argued to be more adequate because it not only controls for the presentation rate, as the many-standards condition does, but also for the

refractoriness of the response and repetition suppression effects due to the predictability of cascade tones (Ruhnau et al., 2012).

The *index of neuronal mismatch* indicates how much a neuron respond to deviant stimuli rather than to standard stimuli (see *Material and methods*); the average for all units was 0.565 ± 0.314. The medians for both RS and FS units were larger than zero (both $p < 0.001$, sign test), and there were no statistical differences *index of neuronal mismatch* between both groups (0.512 ± 0.386 vs 0.584 ± 0.283; $p = 0.414$, Wilcoxon rank-sum test) (Fig. 5A). However, if we analyse each individual AC field, we found that in A1 the *index of neuronal mismatch* of FS units was larger than that of RS units (FS: 0.574 ± 0.268, RS: 0.230 ± 0.270, $p = 0.013$, Wilcoxon rank-sum test). The median *index of neuronal mismatch* was larger than zero in all AC fields for FS units (A1, $p < 0.001$; VAF, $p < 0.001$; AAF, $p = 0.005$; SRAF, $p < 0.001$; PAF, $p < 0.001$), but only in SRAF and PAF for RS units (A1, $p = 0.688$; VAF, $p = 0.065$; AAF, $p = 1.000$; SRAF, $p < 0.001$; PAF, $p = 0.017$). However, there were significant differences in the *index of neuronal mismatch* between the AC fields for RS (Kruskal-Wallis, χ^2 (4, $N = 54$) = 10.91, $p = 0.028$), but not for FS units (Kruskal-Wallis, χ^2 (4, $N = 151$) = 6.93, $p = 0.140$). Post hoc comparisons indicated that the average *index of neuronal mismatch* was significantly lower for RS units in A1 (0.230 ± 0.270) than in PAF or SRAF (0.526 ± 0.534, $p = 0.029$; and 0.626 ± 0.255, $p = 0.021$; respectively) (Fig. 5B).

The *index of repetition suppression* is a measurement of neuronal adaptation to standard stimuli compared to a cascade control sequence (see *Material and methods*); the average for all units was 0.162 ± 0.220. The medians for both RS and FS units were larger than zero (both $p < 0.001$, sign test), and there were no statistical differences *index of repetition suppression* between both groups (0.178 ± 0.300 vs 0.157 ± 0.183; $p = 0.632$ Wilcoxon rank-sum test) (Fig. 5C). Similarly, there were no differences between RS and FS units when looking at each individual AC field. The median *index of repetition suppression* was larger than zero in all AC fields except AAF for FS units (A1, $p < 0.001$; VAF, $p < 0.001$; AAF, $p = 0.262$; SRAF, $p < 0.001$; PAF, $p < 0.020$), but only in SRAF for RS units (A1, $p = 1.000$; VAF, $p = 0.328$; AAF, $p = 1.000$; SRAF, $p = 0.016$; PAF, $p = 0.106$). There were differences in the *index of repetition suppression* among AC fields for RS units (Kruskal-Wallis, χ^2 (4,

$N = 54$) = 9.53, $p = 0.049$) but not for FS units (Kruskal-Wallis, χ^2 (4, $N = 151$) = 7.46, $p = 0.114$) (Fig 5D). However, post hoc comparisons did not find any differences between groups for RS units, although the comparison between A1 and SRAF was close to the level of significance ($p = 0.057$).

The *index of prediction error* indicates how much does a neuron respond to deviant stimuli as compared to a cascade control sequence (see *Material and methods*); the average for all units was 0.403 ± 0.357. The medians for both RS and FS units were larger than zero (both $p < 0.001$, sign test), and there were no statistical differences between both groups (0.335 ± 0.431 vs 0.427 ± 0.324; $p = 0.310$, Wilcoxon rank-sum test) (Fig. 5E). Similarly, there were no differences between RS and FS units when looking at each individual AC field. The median *index of prediction error* was larger than zero in all AC fields except VAF for FS units (A1, $p < 0.001$; VAF, $p = 0.173$; AAF, $p = 0.007$; SRAF, $p < 0.001$; PAF, $p = 0.002$), and in no fields for RS units (A1, $p = 0.328$; VAF, $p = 0.219$; AAF, $p = 1.000$; SRAF, $p = 0.196$; PAF, $p = 0.128$). The *index of prediction error* was similar in all the AC fields, for both RS units (Kruskal-Wallis, χ^2 (4, $N = 54$) = 5.73, $p = 0.220$) and FS units (Kruskal-Wallis, χ^2 (4, $N = 151$) = 1.89, $p = 0.755$) (Fig. 5F).

Altogether, while all the indexes tended to be larger than zero in the individual AC fields for FS units but not for RS units (with the few exceptions indicated before), we only found significant differences between these two types of units in A1. A1 was the only field where the *index of neuronal mismatch* was significantly larger for FS units than for RS units, probably due to a larger *index of prediction error*, which was close to reach statistical significance (FS: 0.453 ± 0.307 vs RS: 0.156 ± 0.370, $p = 0.051$, Wilcoxon rank-sum test).

Given the non-significant differences in the *indexes of repetition suppression* and *prediction error* for RS units between A1 and SRAF/PAF (Fig. 5D,F), it cannot be determined with certainty which of those processes is more relevant to produce a higher *index of neuronal mismatch* in SRAF and PAF than in A1 (Fig. 5B), and therefore, we propose that it is caused by a moderate contribution from each process. Nevertheless, note how RS units in SRAF and PAF tend to have higher *index of prediction error* than A1, which would contribute to higher *index of neuronal mismatch*.

Some studies have proposed that deviance detection and adaptation properties of cortical neurons may be different depending on the layers where they are located (Bastos et al., 2012; Heilbron and Chait, 2018). We compared the distributions of the *indexes of neuronal mismatch*, *repetition suppression* and *prediction error* between supragranular, granular and infragranular layers, but we did not find any statistical differences, neither for all units together (Kruskal-Wallis, χ^2 (2, N = 202) = 2.83, p = 0.243; χ^2 (2, N = 202) = 1.25, p = 0.535; χ^2 (2, N = 202) = 4.23, p = 0.121; respectively for each index) nor when considering RS (Kruskal-Wallis, χ^2 (2, N = 54) = 0.19, p = 0.910; χ^2 (2, N = 54) = 2.00, p = 0.367; χ^2 (2, N = 54) = 0.60, p = 0.742; respectively) or FS units separately (Kruskal-Wallis, χ^2 (2, N = 148) = 3.77, p = 0.152; χ^2 (2, N = 148) = 0.17, p = 0.919; χ^2 (2, N = 148) = 4.50, p = 0. 105; respectively).

4 Discussion

In the present study we compared the deviance detection properties on putative excitatory and inhibitory single units recorded from the AC of anaesthetized rats. Putative inhibitory units had narrower spikes, increased firing rates and smaller spike amplitudes relative to putative excitatory units. While putative inhibitory units spread through all cortical layers, putative excitatory units were mainly confined around layers III–V. Both putative inhibitory and excitatory units showed deviance detection properties, and in both cases the prediction error component was more relevant than repetition suppression.

The AC contains excitatory pyramidal neurons (glutamatergic) and inhibitory interneurons (GABAergic). Excitatory cells comprise ~75% of the neural population and are highly correlated with pyramidal cell morphology (DeFelipe et al., 2013; Douglas and Martin, 2004; Prieto et al., 1994). In the present study, we found a much larger percentage of putative inhibitory than excitatory neurons (74 vs 26%, respectively). This apparent sampling bias does not seem to be related to the cell size (putative excitatory neurons show larger spike amplitudes and SNRs), although the custom-made, high impedance tungsten electrodes that we use may allow us to record rather easily from smaller sized neurons. It is also unlikely to be an effect of the urethane anaesthesia; previous studies have

shown that urethane affects both excitatory and inhibitory currents in a non-selective manner (Hara and Harris, 2002), and it does not alter excitatory glutamate- nor GABA-mediated synaptic transmission (Sceniak and MacIver, 2006).

Contrary to excitatory pyramidal neurons, there is a diversity of inhibitory interneurons, which are usually classified using molecular markers. Inhibitory interneurons seem much more diverse because they may be classified according to different morphological, physiological, molecular, and synaptic properties (e.g., see Ascoli et al., 2008). It is rather common to classify cortical interneurons according to the molecular markers they express, such as the calcium binding protein parvalbumin (PV, which includes chandelier and basket cells), the peptide somatostatin (SOM, such as Martinotti cells) or vasoactive intestinal peptide (VIP, as horse-tail cells). These types comprise the majority of cortical interneurons, although they can be further subdivided using other markers (DeFelipe et al., 2013), and there is also evidence for functionally distinct SOM interneurons (Muñoz et al., 2017). Also, some authors propose that VIP interneurons are a subtype of a larger group which would be characterized by the expression of the ionotropic serotonin receptor 5HT3a (Rudy et al., 2011). VIP neurons inhibit SOM and PV interneurons, and thus participate in a disinhibitory cortical microcircuit (Pi et al., 2013).

After the seminal study from Mountcastle et al. (1969) that proposed that, in general terms, inhibitory and excitatory cortical neurons could be distinguished by the shape of their spikes, other studies have found similar results, adding evidence in support of this type of classification (e.g., Hefti and Smith, 2000; Kawaguchi and Kondo, 2002; Moore and Wehr, 2013). This classification has proven very useful, since it adds relevant information about the function of the units (which is not available using conventional recordings) and can be applied directly to most extracellular recordings (without the need for additional, more complex techniques). It has been successfully used in multiple studies, although with some methodological variations, such as in the references used for measuring the spike widths (e.g., time from peak to trough: Atencio and Schreiner, 2008; half-width, i.e. full width at half-maximal amplitude: Chen et al., 2015; half-valley width: Insel and Barnes, 2015; valley to peak width and half-peak width: Mendoza et al., 2016; Peyrache et al., 2012; width of “after-hyperpolarization”:

Andermann et al., 2004) or the aid of additional dimensions (firing rate, spike amplitude, peak asymmetry, etc.) to refine the classification. Previous studies using a spike width measurement methodology most similar to ours (Barthó et al., 2004; Insel and Barnes, 2015; Mendoza et al., 2016), found that the best spike width cutoff for separating FS and RS would range between ~0.25–0.4 ms (if not considering the other dimensions measured), which is analogous to the 0.35 ms cutoff used here.

The general characteristics of FS and RS units after our classification are in agreement with previous reports. Apart from narrower spike widths, FS units showed increased firing rates and smaller spike amplitudes relative to RS units (Andermann et al., 2004; Atencio and Schreiner, 2008; Baeg et al., 2001; Bruno and Simons, 2002; Calabrese and Woolley, 2015; Chen et al., 2015; Hefti and Smith, 2000; Insel and Barnes, 2015; Mendoza et al., 2016; Moore and Wehr, 2013; Mountcastle et al., 1969; Peyrache et al., 2012). The distribution of FS and RS units across cortical layers differed in some degree from the actual locations of pyramidal neurons and interneurons reported using histological methods (Games and Winer, 1988). While putative inhibitory units were found across all cortical layers (with increased densities in layers II–V) as expected, putative excitatory units were found mainly in layers III–V, peaking at layer IV (Fig. 4B); however, according to histology, pyramidal neurons are very scarce in layer IV. Since the measurement of the recording depth in the present study was based on indirect methods (depth of the recording site as indicated on the microdrive), it is possible that the units estimated to be near the borders between layers could be actually located in the adjacent layer. Considering that layer IV spreads only about 100 μm, a portion of neurons assigned to layer IV could easily be located in layers III or V.

The role of inhibition in the generation of deviance detection responses is still unclear. In subcortical nuclei, it has been shown that GABAergic inhibition has a modulatory effect, acting as a gain control mechanism that enhances and sharpens SSA (Duque et al., 2014; Pérez-González et al., 2012; Pérez-González and Malmierca, 2012). Many studies have found a dependence of MMN on N-methyl-d-aspartate (NMDA) glutamate receptors, which would suggest a relevant role of excitatory cortical neurons in the generation of deviance detection, but we should not ignore the modulatory effect of inhibition on these responses (for a review, see Askew and Metherate, 2016). We found that both FS

and RS units in the AC showed similarly high levels of deviance detection (measured as the *index of neuronal mismatch*, Fig. 5A,B). This finding conforms with previous studies that found that both excitatory and inhibitory (PV and SOM) neurons in the AC exhibit SSA (Chen et al., 2015; Natan et al., 2015). Using whole cell recordings, Chen et al. (2015) found a long latency (mainly subthreshold) component in excitatory neurons, reflecting genuine deviance detection. Interestingly, Natan et al. (2015) found that both types of interneurons contribute to increased SSA in excitatory neurons, but through different mechanisms: optogenetic suppression of SOM interneurons increased the response of excitatory neurons to the standard tones but not to the deviant tones, while suppression of PV interneurons produced an equal increase in the response of excitatory neurons to both standard and deviant tones. The potentially different roles of the various types of inhibitory cortical interneurons are paramount for defining the circuits involved in deviance detection; unfortunately, the methodology of the present study does not allow for the differentiation of subtypes of inhibitory neurons, but it clearly demonstrates that GABAergic neurons play indeed a key role in SSA and deviance detection generation.

The deviance detection properties of both FS and RS units were the result of a high contribution of the prediction error component and reduced repetition suppression. We found that both types of units show similar deviance detection capabilities, as shown by the distributions of *index of neuronal mismatch* (Fig. 5A), and also in both cases the prediction error component (Fig. 5E) has a stronger weight on deviance detection than the repetition suppression component (Fig. 5C). But when looking individually at each field, FS units tended to have average index values different from zero, which was not so common for RS units (Fig. 5B, D, F). Likewise, the distributions of RS and FS units for each field were not different, except for A1 (see below). However, we found some differences in the *index of neuronal mismatch* across AC fields, but only for RS units (Fig. 5B). In this case, the putative excitatory units in A1 (a lemniscal field) showed smaller *index of neuronal mismatch* values compared to units in SRAF and PAF (both of them non-lemniscal fields). This is probably because RS units in SRAF and PAF tend to show larger *index of prediction error* values than RS units in A1, although this trend does not amount to a statistically significant difference. It is noteworthy that A1

was the only AC field where the *index of neuronal mismatch* was different for RS and FS units (Fig. 5B); FS units showed a larger *index of neuronal mismatch* than RS units, maybe due to larger *index of prediction error*. As a lemniscal field, A1 tends to show reduced deviance detection properties compared to non-lemniscal fields (Parras et al., 2017). While FS units from all AC fields have *index of neuronal mismatch* statistically larger than zero, there is a clear distinction between lemniscal (A1, VAF and AAF) and non-lemniscal fields (SRAF, PAF) for RS units. In this group, only non-lemniscal fields have an *index of neuronal mismatch* significantly than zero. These findings suggest that in lemniscal fields mostly FS units contribute to deviance detection, while in non-lemniscal fields both FS and RS units could contribute to the larger deviance detection values found on those areas.

4.1 Limitations

The classification of cortical neurons based on the shape of their spikes is a convenient method that can be implemented on most laboratories performing extracellular recordings; it can even be applied to data retrospectively, as long as they have been stored with enough level of detail. However, this method is indirect, and thus it has some shortcomings. The main limitation may be amount of correspondence between spike shape and neuronal type. Originally, Mountcastle et al. (1969) assigned regular and thin spikes to pyramidal and non-pyramidal cells, respectively. Later studies based both on morphology and cytochemistry have defined a wealth of cortical cell types and subtypes; for instance, Winer (2011) defines 16 different cell types in the auditory cortex. Apart from the pyramidal neurons, also the spiny stellate cells from the granular layers are excitatory. While most inhibitory interneurons are non-pyramidal, there are some exceptions (Budinger and Kanold, 2018; DeFelipe et al., 2013). So, any classification of excitatory/inhibitory neurons based on spike width (alone or accompanied by other measurements) is likely misclassifying a portion of the units.

It can be difficult to estimate how large the deviance detection indexes need to be in order to be functionally significant. As a reference, we can compare the index values found in lemniscal and non-lemniscal AC fields, which are notorious for having different deviance detection capabilities. A previous study, using methods comparable to those used here, found that the median *index of neuronal mismatch* only differed 0.10 between lemniscal and non-lemniscal AC fields (0.50 vs 0.60,

Parras et al., 2017). Hence, relatively small differences in this index may imply substantial physiological distinctions. In the present study, the difference in the median values of the *index of neuronal mismatch* between RS and FS units is only 0.04 (0.60 vs 0.64, respectively, Fig. 5A), maybe too small to be functionally relevant. On the other hand, if we look into A1, the difference reaches 0.38 (0.25 vs 0.63, Fig. 5B). This suggests that taking all AC units as a whole, the deviance detection sensitivity of RS and FS units appears to be very similar, whereas in some particular areas the differences could be quite substantial.

The use of modern techniques, such as optogenetics or two-photon microscopy, allowing the selective activation/inactivation or the labelling of known cell types while recording from those neurons, may decrease the current uncertainties of using this classification.

5 Conclusions

Measurements of spike widths in extracellular recordings from the anesthetized rat AC can be used to classify the units as putative excitatory or inhibitory. This classification adds a layer of information to the neuronal activity recorded, which is unavailable using basic extracellular electrophysiology methods. In a set of recordings obtained in response to an auditory oddball paradigm, we found that both putative excitatory and inhibitory neurons in the rat AC show similar levels of deviance detection. When comparing the responses to the oddball paradigm to the responses to the corresponding control sequences, and interpreting the results under the predictive coding framework, we found that the responses of both types of neurons reflect a predominance of the prediction error signalling rather than repetition suppression. Altogether, the results obtained in this study suggest the involvement of both types of neurons in the circuits that generate deviance detection.

Author contributions

Data collection and curation: GGP, CJMD, CA, GVC. Conceptualization, experimental design and writing: MSM and DPG. Data analysis: DPG. Funding acquisition: MSM.

Acknowledgements

This work was supported by a Spanish MINECO Grant (SAF2016-75803-P) to MSM and a Juan de la Cierva Fellowship (FJCI-2016-27897) to CJMD.

References

Andermann, M.L., Ritt, J., Neimark, M.A., Moore, C.I., 2004. Neural correlates of vibrissa resonance: Band-pass and somatotopic representation of high-frequency stimuli. Neuron 42, 451–463. https://doi.org/10.1016/S0896-6273(04)00198-9

Anderson, L.A., Malmierca, M.S., 2013. The effect of auditory cortex deactivation on stimulus-specific adaptation in the inferior colliculus of the rat. Eur. J. Neurosci. 37, 52–62. https://doi.org/10.1111/ejn.12018

Antunes, F.M., Malmierca, M.S., 2014. An overview of stimulus-specific adaptation in the auditory thalamus. Brain Topogr. 27, 480–499. https://doi.org/10.1007/s10548-013-0342-6

Antunes, F.M., Nelken, I., Covey, E., Malmierca, M.S., 2010. Stimulus-specific adaptation in the auditory thalamus of the anesthetized rat. PLoS One 5, e14071. https://doi.org/10.1371/journal.pone.0014071

Ascoli, G.A., Alonso-Nanclares, L., Anderson, S.A., Barrionuevo, G., Benavides-Piccione, R., Burkhalter, A., Buzsáki, G., Cauli, B., DeFelipe, J., Fairén, A., Feldmeyer, D., Fishell, G., Fregnac, Y., Freund, T.F., Gardner, D., Gardner, E.P., Goldberg, J.H., Helmstaedter, M., Hestrin, S., Karube, F., Kisvárday, Z.F., Lambolez, B., Lewis, D.A., Marin, O., Markram, H., Mũoz, A., Packer, A., Petersen, C.C.H., Rockland, K.S., Rossier, J., Rudy, B., Somogyi, P., Staiger, J.F., Tamas, G., Thomson, A.M., Toledo-Rodriguez, M., Wang, Y., West, D.C., Yuste, R., 2008. Petilla terminology: Nomenclature of features of GABAergic interneurons of the cerebral cortex. Nat. Rev. Neurosci. 9, 557–568. https://doi.org/10.1038/nrn2402

Askew, C.E., Metherate, R., 2016. Synaptic interactions and inhibitory regulation in auditory cortex. Biol. Psychol. 116, 4–9. https://doi.org/10.1016/j.biopsycho.2015.11.001

Atencio, C.A., Schreiner, C.E., 2008. Spectrotemporal processing differences between auditory

cortical fast-spiking and regular-spiking neurons. J. Neurosci. 28, 3897–3910. https://doi.org/10.1523/JNEUROSCI.5366-07.2008

Ayala, Y.A., Malmierca, M.S., 2013. Stimulus-specific adaptation and deviance detection in the inferior colliculus. Front. Neural Circuits 6, 89. https://doi.org/10.3389/fncir.2012.00089

Ayala, Y.A., Pérez-González, D., Duque, D., Nelken, I., Malmierca, M.S., 2013. Frequency discrimination and stimulus deviance in the inferior colliculus and cochlear nucleus. Front. Neural Circuits 6, 119. https://doi.org/10.3389/fncir.2012.00119

Ayala, Y.A., Pérez-González, D., Malmierca, M.S., 2016. Stimulus-specific adaptation in the inferior colliculus: The role of excitatory, inhibitory and modulatory inputs. Biol. Psychol. 116, 10–22. https://doi.org/10.1016/j.biopsycho.2015.06.016

Ayala, Y.A., Udeh, A., Dutta, K., Bishop, D., Malmierca, M.S., Oliver, D.L., 2015. Differences in the strength of cortical and brainstem inputs to SSA and non-SSA neurons in the inferior colliculus. Sci. Rep. 5, 1–17. https://doi.org/10.1038/srep10383

Baeg, E.H., Kim, B.K., Jang, J., Kim, H.T., Mook-Jung, I., Jung, M.W., 2001. Fast Spiking and Regular Spiking Neural Correlates of Fear Conditioning in the Medial Prefrontal Cortex of the Rat. Cereb. Cortex 11, 441–451. https://doi.org/10.1093/cercor/11.5.441

Barthó, P., Hirase, H., Monconduit, L., Zugaro, M., Harris, K.D., Buzsáki, G., 2004. Characterization of neocortical principal cells and interneurons by network interactions and extracellular features. J. Neurophysiol. 92, 600–608. https://doi.org/10.1152/jn.01170.2003

Bastos, A.M., Usrey, W.M., Adams, R.A., Mangun, G.R., Fries, P., Friston, K.J., 2012. Canonical Microcircuits for Predictive Coding. Neuron 76, 695–711. https://doi.org/10.1016/j.neuron.2012.10.038

Bruno, R.M., Simons, D.J., 2002. Feedforward mechanisms of excitatory and inhibitory cortical receptive fields. J. Neurosci. 22, 10966–10975.

Budinger, E., Kanold, P.O., 2018. Auditory Cortex Circuits, in: Oliver, D.L., Cant, N.B., Fay, R.R., Popper, A.N. (Eds.), The Mammalian Auditory Pathways: Synaptic Organization and Microcircuits. Springer, pp. 199–233. https://doi.org/10.1007/978-3-319-71798-2_8

Calabrese, A., Woolley, S.M.N., 2015. Coding principles of the canonical cortical microcircuit in the avian brain. Proc. Natl. Acad. Sci. 112, 3517–3522. https://doi.org/10.1073/pnas.1408545112

Carbajal, G. V., Malmierca, M.S., 2018. The Neuronal Basis of Predictive Coding Along the Auditory Pathway: From the Subcortical Roots to Cortical Deviance Detection. Trends Hear. 22, 233121651878482. https://doi.org/10.1177/2331216518784822

Casado-Román, L., Pérez-González, D., Malmierca, M.S., 2019. Prediction errors explain mismatch signals of neurons in the medial prefrontal cortex. bioRxiv 778928. https://doi.org/10.1101/778928

Chen, I.W., Helmchen, F., Lütcke, H., 2015. Specific early and late oddball-evoked responses in excitatory and inhibitory neurons of mouse auditory cortex. J. Neurosci. 35, 12560–12573. https://doi.org/10.1523/JNEUROSCI.2240-15.2015

DeFelipe, J., López-Cruz, P.L., Benavides-Piccione, R., Bielza, C., Larrañaga, P., Anderson, S., Burkhalter, A., Cauli, B., Fairén, A., Feldmeyer, D., Fishell, G., Fitzpatrick, D., Freund, T.F., González-Burgos, G., Hestrin, S., Hill, S., Hof, P.R., Huang, J., Jones, E.G., Kawaguchi, Y., Kisvárday, Z., Kubota, Y., Lewis, D.A., Marín, O., Markram, H., McBain, C.J., Meyer, H.S., Monyer, H., Nelson, S.B., Rockland, K., Rossier, J., Rubenstein, J.L.R., Rudy, B., Scanziani, M., Shepherd, G.M., Sherwood, C.C., Staiger, J.F., Tamás, G., Thomson, A., Weng, Y., Yuste, R., Ascoli, G.A., 2013. New insights into the classification and nomenclature of cortical

GABAergic interneurons. Nat. Rev. Neurosci. 14, 202–216. https://doi.org/10.1038/nrn3444

Douglas, R.J., Martin, K.A.C., 2004. Neuronal circuits of the neocortex. Annu. Rev. Neurosci. 27, 419–451. https://doi.org/10.1146/annurev.neuro.27.070203.144152

Duque, D., Malmierca, M.S., Caspary, D.M., 2014. Modulation of stimulus-specific adaptation by GABAA receptor activation or blockade in the medial geniculate body of the anaesthetized rat. J. Physiol. 592, 729–743. https://doi.org/10.1113/jphysiol.2013.261941

Duque, D., Perez-Gonzalez, D., Ayala, Y.A., Palmer, A.R., Malmierca, M.S., 2012. Topographic Distribution, Frequency, and Intensity Dependence of Stimulus-Specific Adaptation in the Inferior Colliculus of the Rat. J. Neurosci. 32, 17762–17774. https://doi.org/10.1523/JNEUROSCI.3190-12.2012

Friston, K., 2005. A theory of cortical responses. Philos. Trans. R. Soc. B Biol. Sci. 360, 815–836. https://doi.org/10.1098/rstb.2005.1622

Games, K.D., Winer, J.A., 1988. Layer V in rat auditory cortex: Projections to the inferior colliculus and contralateral cortex. Hear. Res. 34, 1–25. https://doi.org/10.1016/0378-5955(88)90047-0

Garrido, M.I., Kilner, J.M., Stephan, K.E., Friston, K.J., 2009. The mismatch negativity: A review of underlying mechanisms. Clin. Neurophysiol. 120, 453–463. https://doi.org/10.1016/j.clinph.2008.11.029

Hara, K., Harris, R.A., 2002. The anesthetic mechanism of urethane: the effects on neurotransmitter-gated ion channels. Anesth Analg 94, 313–318.

Hefti, B.J., Smith, P.H., 2000. Anatomy, physiology, and synaptic responses of rat layer V auditory cortical cells and effects of intracellular GABA(A) blockade. J. Neurophysiol. 83, 2626–2638. https://doi.org/10.1152/jn.2000.83.5.2626

Heilbron, M., Chait, M., 2018. Great Expectations: Is there Evidence for Predictive Coding in Auditory Cortex? Neuroscience 389, 54–73. https://doi.org/10.1016/j.neuroscience.2017.07.061

Insel, N., Barnes, C.A., 2015. Differential activation of fast-spiking and regular-firing neuron populations during movement and reward in the dorsal medial frontal cortex. Cereb. Cortex 25, 2631–2647. https://doi.org/10.1093/cercor/bhu062

Kawaguchi, Y., Kondo, S., 2002. Parvalbumin, somatostatin and cholecystokinin as chemical markers for specific GABAergic interneuron types in the rat frontal cortex. J. Neurocytol. 31, 277–287. https://doi.org/10.1023/A:1024126110356

Kostal, L., Lansky, P., Stiber, M., 2018. Statistics of inverse interspike intervals: The instantaneous firing rate revisited. Chaos 28, 1–8. https://doi.org/10.1063/1.5036831

Malmierca, M.S., 2015. Auditory System, in: Paxinos, G. (Ed.), The Rat Nervous System. Elsevier - Academic Press, pp. 865–946.

Malmierca, M.S., Anderson, L.A., Antunes, F.M., 2015. The cortical modulation of stimulus-specific adaptation in the auditory midbrain and thalamus: a potential neuronal correlate for predictive coding. Front. Syst. Neurosci. 9, 1–14. https://doi.org/10.3389/fnsys.2015.00019

Malmierca, M.S., Cristaudo, S., Pérez-González, D., Covey, E., 2009. Stimulus-specific adaptation in the inferior colliculus of the anesthetized rat. J. Neurosci. 29, 5483–5493. https://doi.org/10.1523/JNEUROSCI.4153-08.2009

Mendoza, G., Peyrache, A., Gámez, J., Prado, L., Buzsáki, G., Merchant, H., 2016. Recording extracellular neural activity in the behaving monkey using a semichronic and high-density electrode system. J. Neurophysiol. 116, 563–574. https://doi.org/10.1152/jn.00116.2016

Michie, P.T., Malmierca, M.S., Harms, L., Todd, J., 2016a. The neurobiology of MMN and

implications for schizophrenia. Biol. Psychol. 116, 90–97. https://doi.org/10.1016/j.biopsycho.2016.01.011

Michie, P.T., Malmierca, M.S., Harms, L., Todd, J., 2016b. Understanding the neurobiology of MMN and its reduction in schizophrenia. Biol. Psychol. 116, 1–3. https://doi.org/10.1016/j.biopsycho.2016.02.005

Moore, A.K., Wehr, M., 2013. Parvalbumin-Expressing Inhibitory Interneurons in Auditory Cortex Are Well-Tuned for Frequency. J. Neurosci. 33, 13713–13723. https://doi.org/10.1523/JNEUROSCI.0663-13.2013

Mountcastle, V.B., Talbot, W.H., Sakata, H., Hyvärinen, J., 1969. Cortical neuronal mechanisms in flutter-vibration studied in unanesthetized monkeys. Neuronal periodicity and frequency discrimination. J. Neurophysiol. 32, 452–484. https://doi.org/10.1152/jn.1969.32.3.452

Muñoz, W., Tremblay, R., Levenstein, D., Rudy, B., 2017. Layer-specific modulation of neocortical dendritic inhibition during active wakefulness. Science (80-.). 355, 954–959. https://doi.org/10.1126/science.aag2599

Näätänen, R., Gaillard, A.W., Mantysalo, S., 1978. Early selective-attention effect on evoked potential reinterpreted. Acta Psychol 42, 313–329.

Näätänen, R., Kujala, T., Escera, C., Baldeweg, T., Kreegipuu, K., Carlson, S., Ponton, C., 2012. The mismatch negativity (MMN) - A unique window to disturbed central auditory processing in ageing and different clinical conditions. Clin. Neurophysiol. 123, 424–458. https://doi.org/10.1016/j.clinph.2011.09.020

Natan, R.G., Briguglio, J.J., Mwilambwe-Tshilobo, L., Jones, S.I., Aizenberg, M., Goldberg, E.M., Geffen, M.N., 2015. Complementary control of sensory adaptation by two types of cortical interneurons. Elife 4, 1–27. https://doi.org/10.7554/eLife.09868

Nieto-Diego, J., Malmierca, M.S., 2016. Topographic Distribution of Stimulus-Specific Adaptation across Auditory Cortical Fields in the Anesthetized Rat. PLoS Biol. 14, 1–30. https://doi.org/10.1371/journal.pbio.1002397

Pandya, P.K., Rathbun, D.L., Moucha, R., Engineer, N.D., Kilgard, M.P., 2008. Spectral and temporal processing in rat posterior auditory cortex. Cereb. Cortex 18, 301–314. https://doi.org/10.1093/cercor/bhm055

Parras, G.G., Nieto-Diego, J., Carbajal, G. V., Valdés-Baizabal, C., Escera, C., Malmierca, M.S., 2017. Neurons along the auditory pathway exhibit a hierarchical organization of prediction error. Nat. Commun. 8. https://doi.org/10.1038/s41467-017-02038-6

Parras, G.G., Valdés-Baizabal, C., Harms, L., Michie, P., Malmierca, M.S., 2019. The effect of NMDA-R antagonist, MK-801, on neuronal mismatch along the auditory thalamocortical pathway. bioRxiv 636068. https://doi.org/10.1101/636068

Pérez-González, D., Hernández, O., Covey, E., Malmierca, M.S., 2012. GABA(A)-mediated inhibition modulates stimulus-specific adaptation in the inferior colliculus. PLoS One 7, e34297. https://doi.org/10.1371/journal.pone.0034297

Pérez-González, D., Malmierca, M.S., 2014. Adaptation in the auditory system: an overview. Front. Integr. Neurosci. 8, 19. https://doi.org/10.3389/fnint.2014.00019

Pérez-González, D., Malmierca, M.S., 2012. Variability of the time course of stimulus-specific adaptation in the inferior colliculus. Front. Neural Circuits 6. https://doi.org/10.3389/fncir.2012.00107

Pérez-González, D., Malmierca, M.S., Covey, E., 2005. Novelty detector neurons in the mammalian auditory midbrain. Eur. J. Neurosci. 22, 2879–2885. https://doi.org/10.1111/j.1460-9568.2005.04472.x

Peyrache, A., Dehghani, N., Eskandar, E.N., Madsen, J.R., Anderson, W.S., Donoghue, J.A., Hochberg, L.R., Halgren, E., Cash, S.S., Destexhe, A., 2012. Spatiotemporal dynamics of neocortical excitation and inhibition during human sleep. Proc. Natl. Acad. Sci. U. S. A. 109, 1731–1736. https://doi.org/10.1073/pnas.1109895109

Pi, H.J., Hangya, B., Kvitsiani, D., Sanders, J.I., Huang, Z.J., Kepecs, A., 2013. Cortical interneurons that specialize in disinhibitory control. Nature 503, 521–524. https://doi.org/10.1038/nature12676

Polley, D.B., Read, H.L., Storace, D.A., Merzenich, M.M., 2007. Multiparametric auditory receptive field organization across five cortical fields in the albino rat. J. Neurophysiol. 97, 3621–3638. https://doi.org/10.1152/jn.01298.2006

Prieto, J.J., Peterson, B.A., Winer, J.A., 1994. Morphology and spatial distribution of GABAergic neurons in cat primary auditory cortex (AI). J. Comp. Neurol. 344, 349–382. https://doi.org/10.1002/cne.903440304

Profant, O., Burianová, J., Syka, J., 2013. The response properties of neurons in different fields of the auditory cortex in the rat. Hear. Res. 296, 51–59. https://doi.org/10.1016/j.heares.2012.11.021

Rudy, B., Fishell, G., Lee, S.H., Hjerling-Leffler, J., 2011. Three groups of interneurons account for nearly 100% of neocortical GABAergic neurons. Dev. Neurobiol. 71, 45–61. https://doi.org/10.1002/dneu.20853

Ruhnau, P., Herrmann, B., Schröger, E., 2012. Finding the right control: The mismatch negativity under investigation. Clin. Neurophysiol. 123, 507–512. https://doi.org/10.1016/j.clinph.2011.07.035

Sceniak, M.P., MacIver, M.B., 2006. Cellular actions of urethane on rat visual cortical neurons in vitro. J. Neurophysiol. 95, 3865–3874. https://doi.org/10.1152/jn.01196.2005

Smith, P.H., Uhlrich, D.J., Manning, K.A., Banks, M.I., 2012. Thalamocortical projections to rat auditory cortex from the ventral and dorsal divisions of the medial geniculate nucleus. J. Comp. Neurol. 520, 34–51. https://doi.org/10.1002/cne.22682

Tsolaki, A.C., Kosmidou, V., Kompatsiaris, I. (Yiannis), Papadaniil, C., Hadjileontiadis, L., Adam, A., Tsolaki, M., 2017. Brain source localization of MMN and P300 ERPs in mild cognitive impairment and Alzheimer's disease: a high-density EEG approach. Neurobiol. Aging 55, 190–201. https://doi.org/10.1016/j.neurobiolaging.2017.03.025

Ulanovsky, N., Las, L., Nelken, I., 2003. Processing of low-probability sounds by cortical neurons. Nat. Neurosci. 6, 391–398. https://doi.org/10.1038/nn1032

Vlaskamp, C., Oranje, B., Madsen, G.F., Møllegaard Jepsen, J.R., Durston, S., Cantio, C., Glenthøj, B., Bilenberg, N., 2017. Auditory processing in autism spectrum disorder: Mismatch negativity deficits. Autism Res. 10, 1857–1865. https://doi.org/10.1002/aur.1821

Wiens, S., Szychowska, M., Eklund, R., van Berlekom, E., 2019. Cascade and no-repetition rules are comparable controls for the auditory frequency mismatch negativity in oddball tasks. Psychophysiology 56, 1–12. https://doi.org/10.1111/psyp.13280

Winer, J.A., 2011. Neurochemical Organization of the Medial Geniculate Body and Auditory Cortex, in: Winer, J.A., Schreiner, C.E. (Eds.), The Auditory Cortex. Springer, New York, pp. 209–234.

Winer, J.A., Sally, S.L., Larue, D.T., Kelly, J.B., 1999. Origins of medial geniculate body projections to physiologically defined zones of rat primary auditory cortex. Hear. Res. 130, 42–61. https://doi.org/10.1016/S0378-5955(98)00217-2

Figure legends

Figure 1: Spike width measurement. A) The spikes for each isolated unit were aligned on the trough. The mean (black solid line) and standard deviation (dotted black lines) of the spikes of each unit was calculated. Based on the mean waveform, we measured the peak-to-trough amplitude (vertical line) and spike half-width (spike width at 50% of the peak-to-trough amplitude). **B)** Distribution of the peak-to-trough signal to noise ratio (SNR). Only units with an SNR > 5 were included in the study (dotted line). **C)** Distribution of the number of spikes per unit. About 95% of the units included more than 200 spikes.

Figure 2: Classification of units based on spike width and firing rate. A) Distribution of spike widths measured in our sample. Units with a spike width larger than 0.35 ms (dashed grey line) were classified as regular spiking (RS, orange), while the rest were classified as fast spiking (FS, blue). **B)** Violin plot showing the distribution of spike widths in RS and FS units. In this and similar violin plots, the horizontal solid line indicates the mean of the distribution, while the white circle indicates the median. The thick grey bar expands from the first (Q1) to the third quartile (Q3), and the whiskers show the range of lower and higher adjacent values (i.e. values within 1.5 IQR below Q1 or above Q3, respectively). The triangles indicate a 95% confidence interval for the median. **C)** The instantaneous firing rate (median ± 95% confidence interval) was significantly lower for RS than for FS units for the 25^{th}, 10^{th} (**$p<0.01$), 5^{th} and 1^{st} percentiles (***$p<0.001$), but not for the 50^{th} percentile.

Figure 3: Location of RS and FS units in AC cortical fields and spike amplitude. A) Number and percentage of RS (orange) and FS (blue) units located in the primary AC (A1), ventral auditory field (VAF), anterior auditory field (AAF), suprarhinal auditory field (SRAF) and posterior auditory field (PAF). **B)** Distribution of spike widths in RS and FS units for each auditory field. There were no significant differences in the distribution of spike widths across fields for neither RS nor FS units. **C)** Distribution spike amplitudes for RS and FS units. The amplitude of RS units was significantly larger than that of FS units (***$p<0.001$). **D)** Distribution of spike amplitudes in RS and FS units for each

auditory field. There were no significant differences in the distribution of spike amplitudes across fields for neither RS nor FS units.

Figure 4: Location of RS and FS units in cortical layers. A) Depth of the recording sites for RS and FS units. **B)** Left side: density of RS and FS units per layer, calculated as number of units per 100 μm (n = 202). RS units were most commonly found in layers IV–V, while FS units spread over layers II–V. Right side: density of RS and FS units in supragranular (I–III) and infragranular (V–IV) layers. **C)** Distribution of recording site depths of RS and FS units for each auditory field. There were no significant differences in the distribution of spike amplitudes across fields for FS units nor for RS units. Approximate cortical layer depths (I−VI) based on Games and Winer (1988).

Figure 5: Indexes of Neuronal Mismatch, Repetition Suppression and Prediction Error. A,B) Distribution of the *index of neuronal mismatch* of RS and FS units for each auditory field. **C,D)** Distribution of the *index of repetition suppression* of RS and FS units for each auditory field. **E,F)** Distribution of the *index of prediction error* of RS and FS units for each auditory field. Asterisks above the violin plots indicate that the group average is different from zero; brackets indicate differences between groups (*p<0.05, **p<0.01, ***p<0.001).

Supplementary Figure 1: Firing rates of RS and FS units. A-E) Left panels: Distribution of several percentiles (50^{th}, 25^{th}, 10^{th}, 5^{th} and 1^{st}) of instantaneous firing rates for RS (orange) and FS (blue) units, compared to the spike width measured for each unit. Right panels: violin plots showing the distribution of instantaneous firing rates for RS and FS units.

Supplementary Figure 2: Signal-to-noise ratio (SNR) of RS and FS units. A) Distribution of SNR for RS (orange) and FS (blue) units. The SNR of RS units was significantly larger than that of FS units (***p<0.001). **B)** Distribution of SNR in RS and FS units for each auditory field. There were no significant differences in the distribution of SNR across fields for neither RS nor FS units.

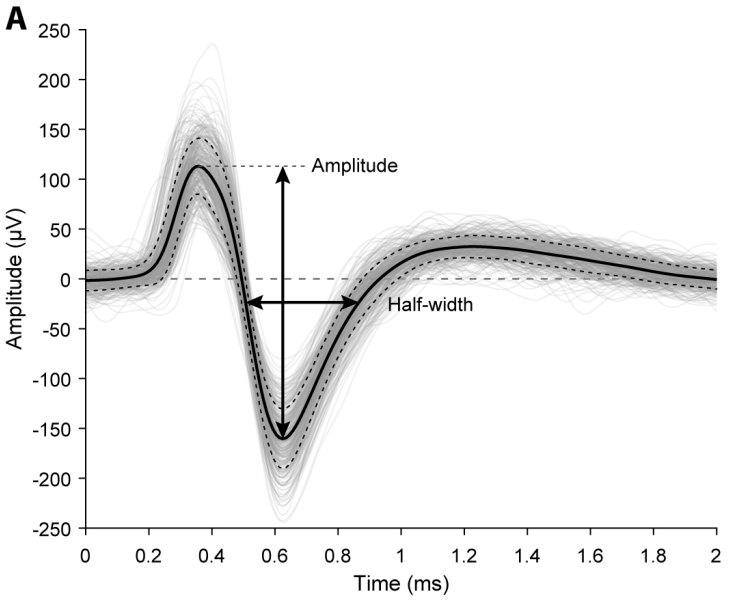
A
Amplitude
Half-width
Amplitude (μV)
Time (ms)
250
200
150
100
50
0
-50
-100
-150
-200
-250
0
0.2
0.4
0.6
0.8
1
1.2
1.4
1.6
1.8
2

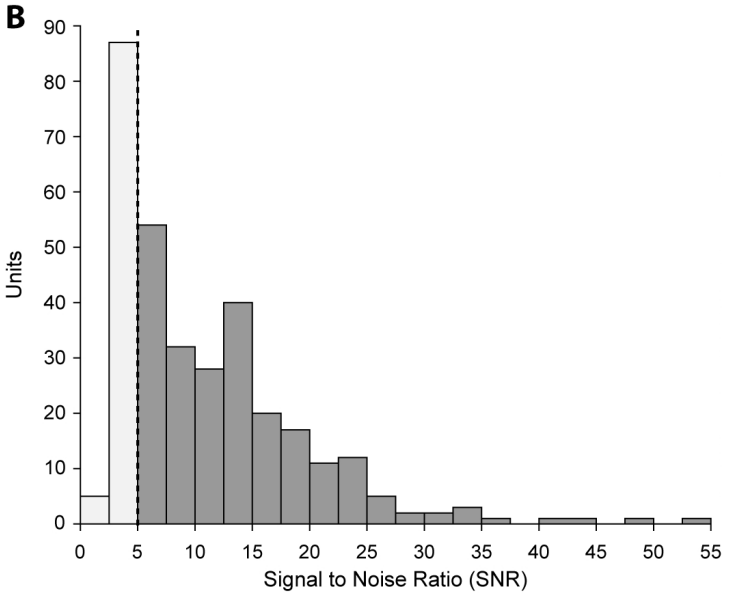
B
Units
Signal to Noise Ratio (SNR)
90
80
70
60
50
40
30
20
10
0
0
5
10
15
20
25
30
35
40
45
50
55

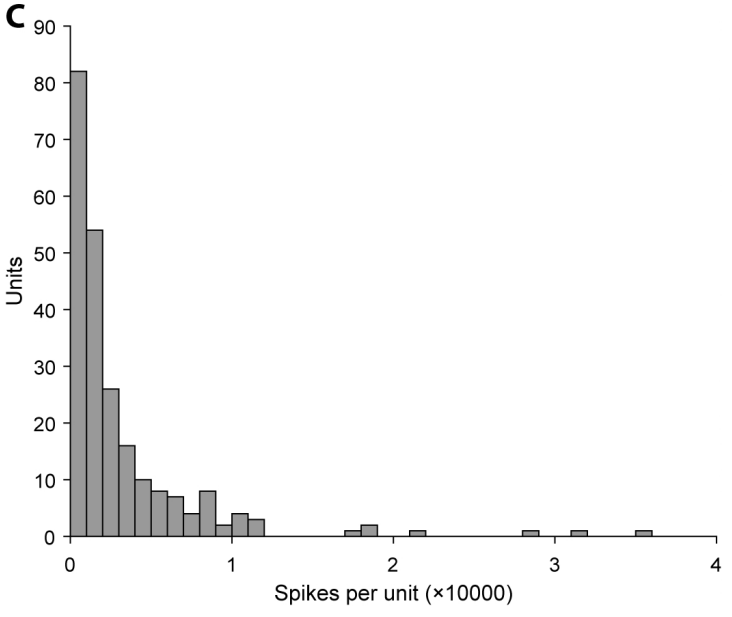
C
Units
Spikes per unit (×10000)
90
80
70
60
50
40
30
20
10
0
0
1
2
3
4

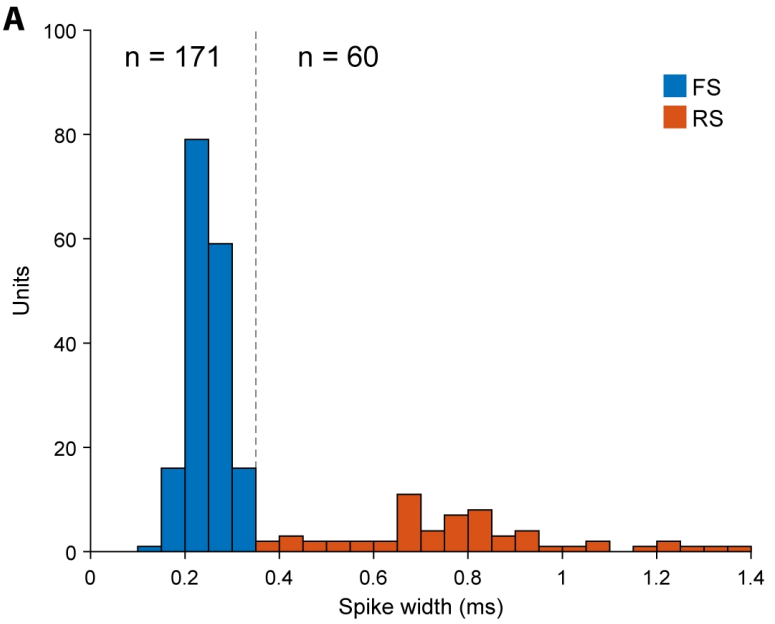
A
n = 171
n = 60
FS
RS
Units
Spike width (ms)

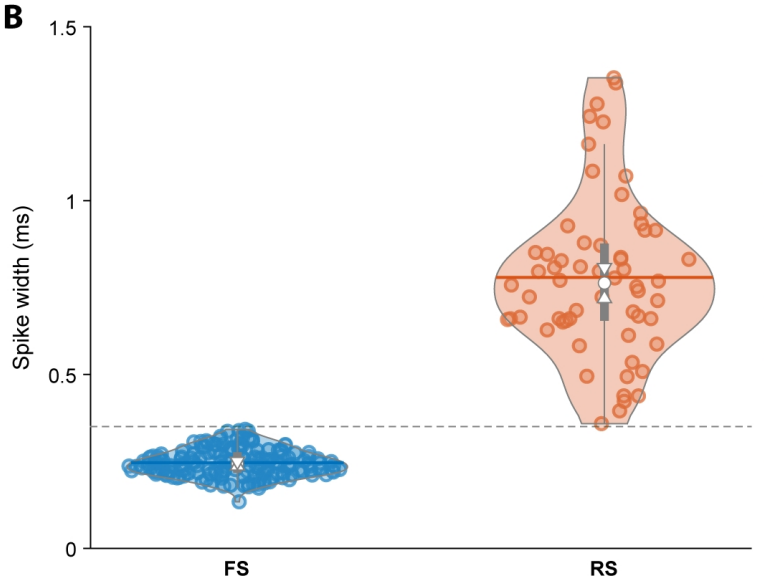
B
Spike width (ms)
FS
RS

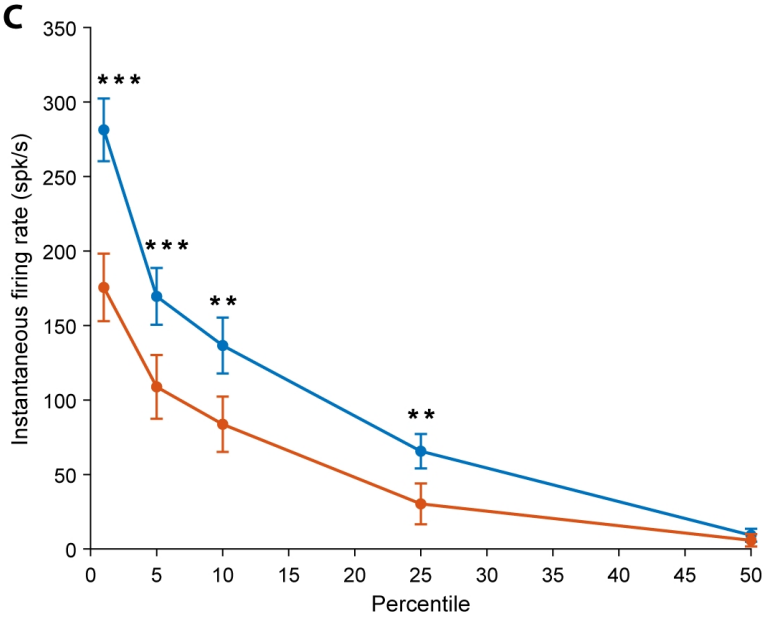
C
Instantaneous firing rate (spk/s)
Percentile

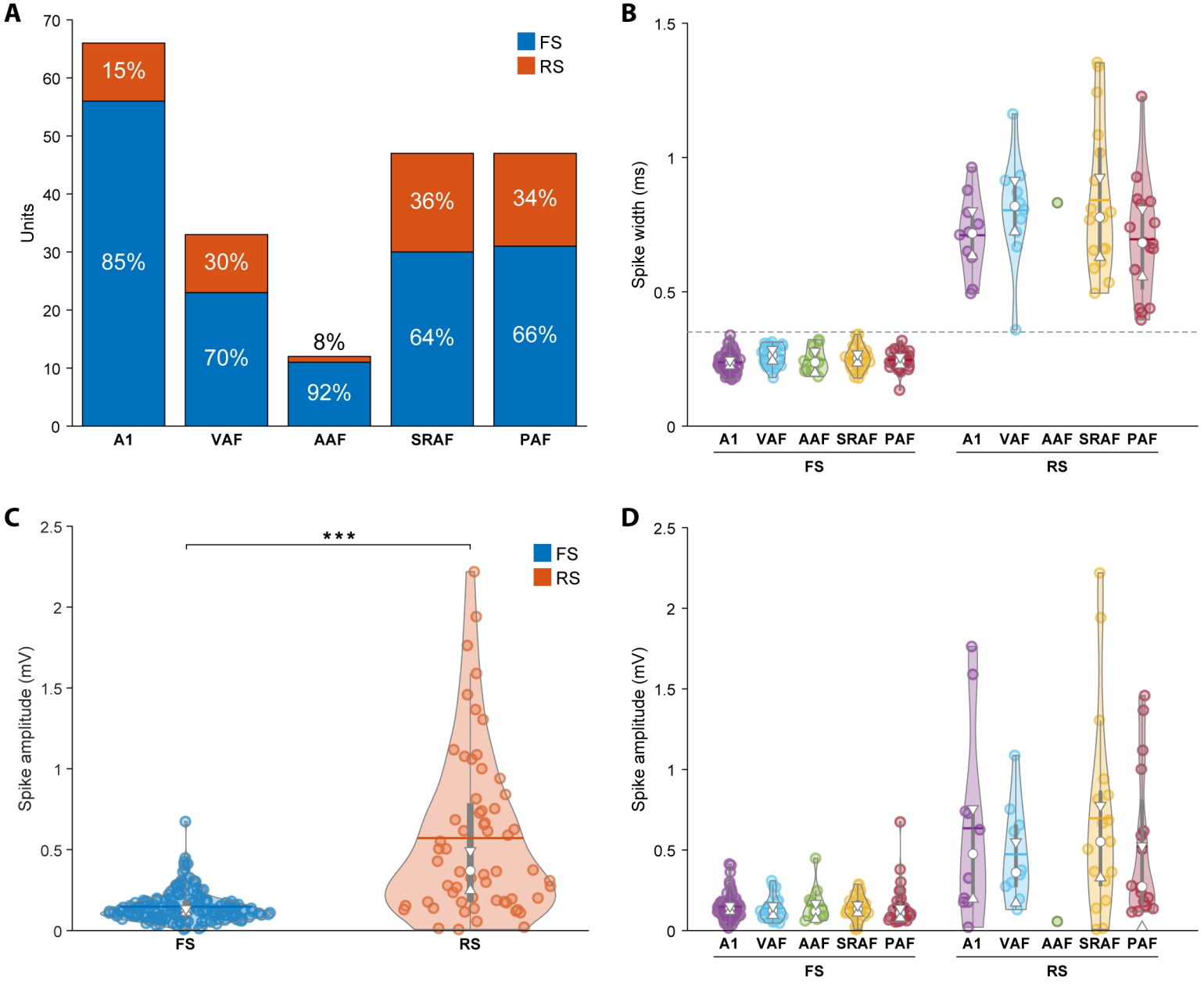
A
B
C
D
Units
FS
RS
15%
85%
30%
70%
8%
92%
36%
64%
34%
66%
A1
VAF
AAF
SRAF
PAF
Spike width (ms)
Spike amplitude (mV)
***

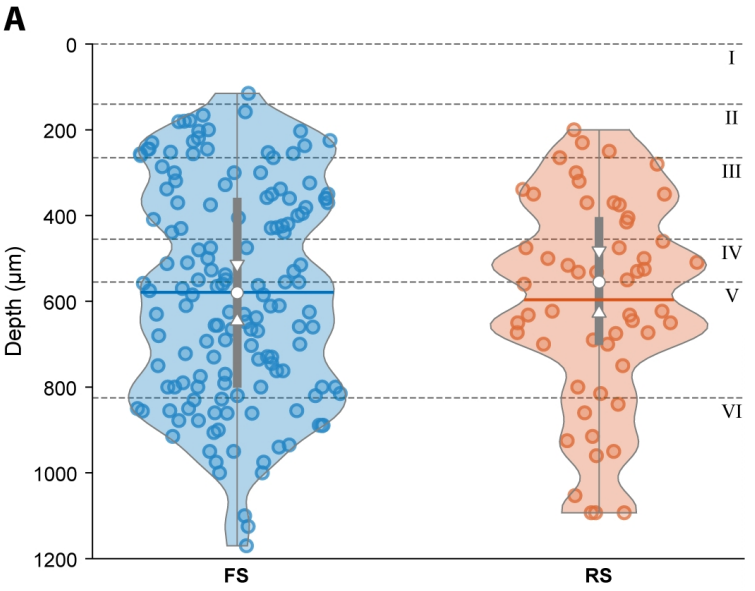
A
Depth (µm)
0
200
400
600
800
1000
1200
I
II
III
IV
V
VI
FS
RS

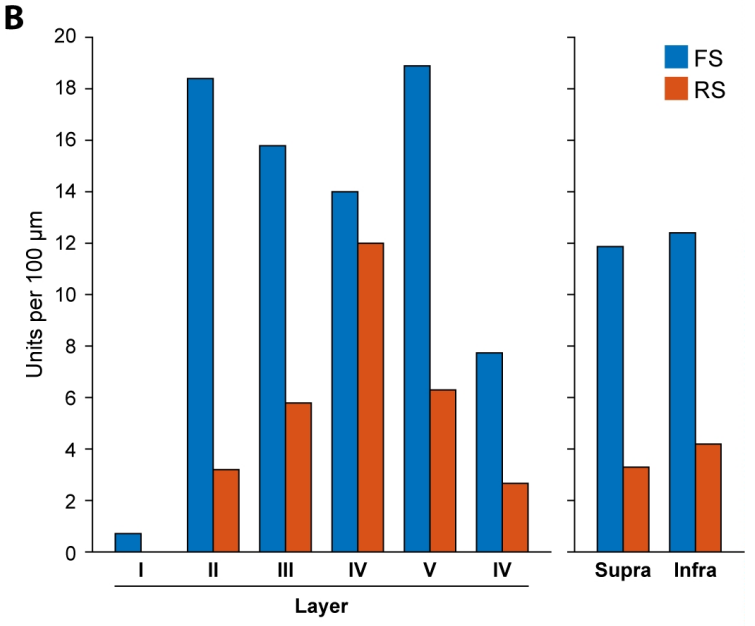
B
Units per 100 µm
0
2
4
6
8
10
12
14
16
18
20
FS
RS
I
II
III
IV
V
IV
Supra
Infra
Layer

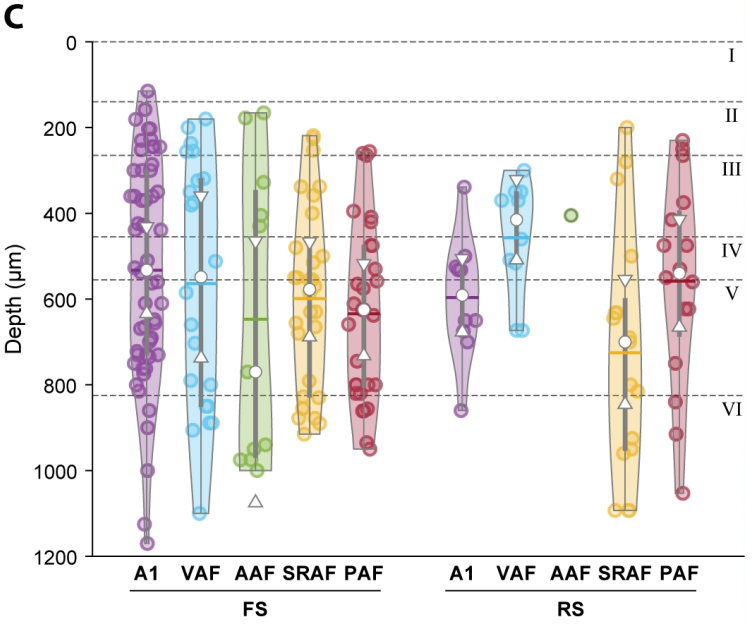
C
Depth (µm)
0
200
400
600
800
1000
1200
I
II
III
IV
V
VI
A1
VAF
AAF
SRAF
PAF
FS
A1
VAF
AAF
SRAF
PAF
RS

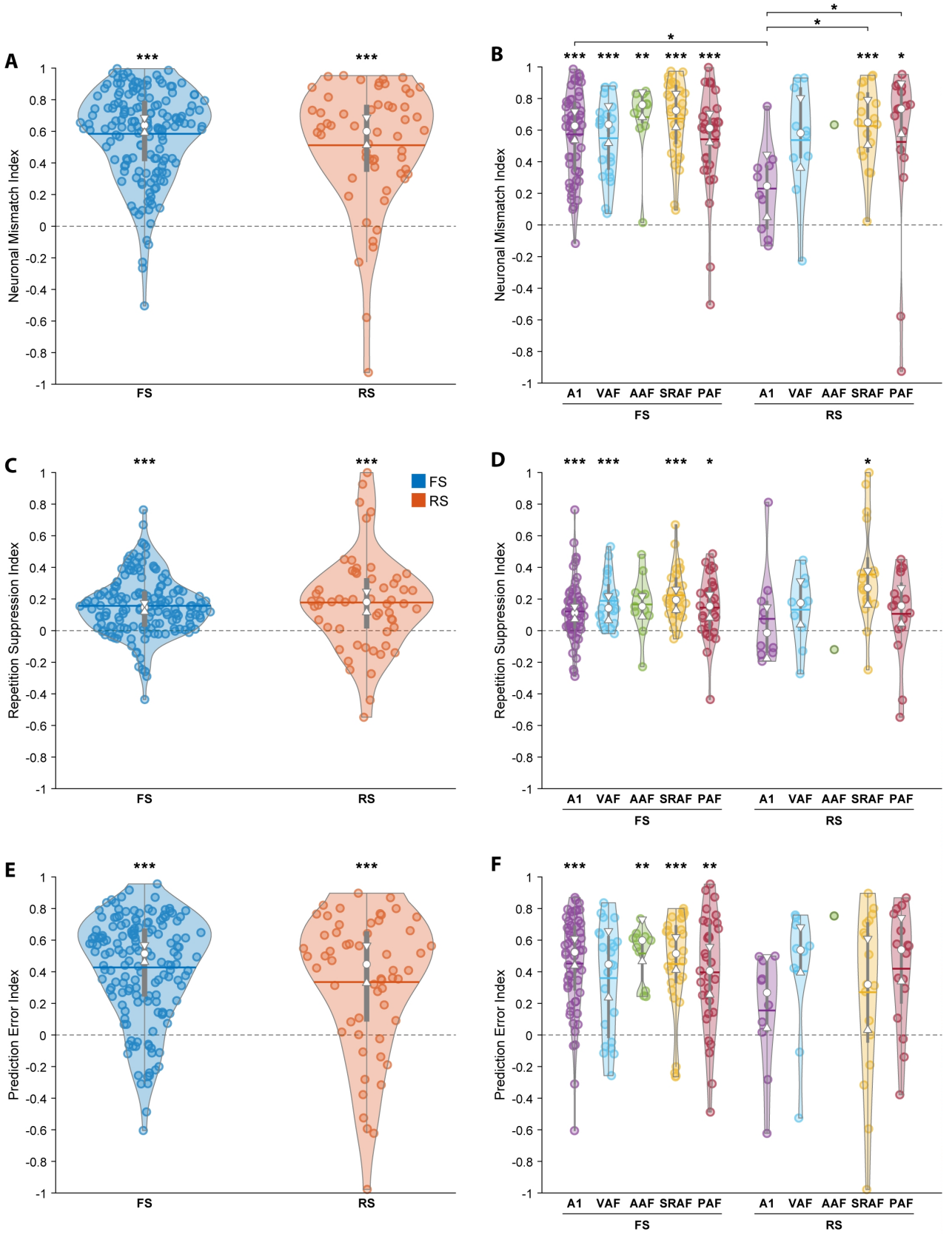
A
B
C
D
E
F
Neuronal Mismatch Index
Repetition Suppression Index
Prediction Error Index
FS
RS
A1
VAF
AAF
SRAF
PAF

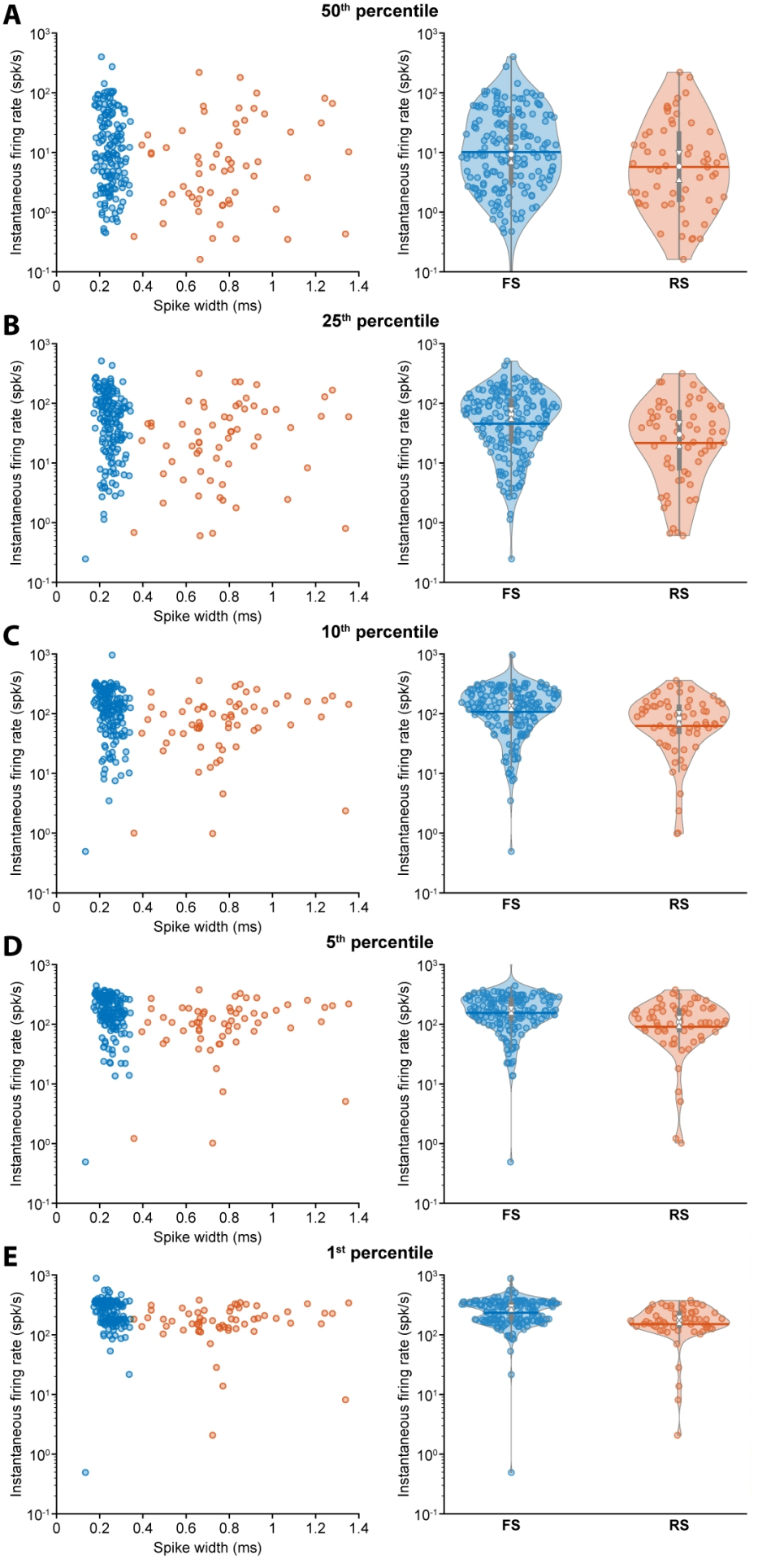
A
50th percentile
B
25th percentile
C
10th percentile
D
5th percentile
E
1st percentile
Instantaneous firing rate (spk/s)
Spike width (ms)
FS
RS

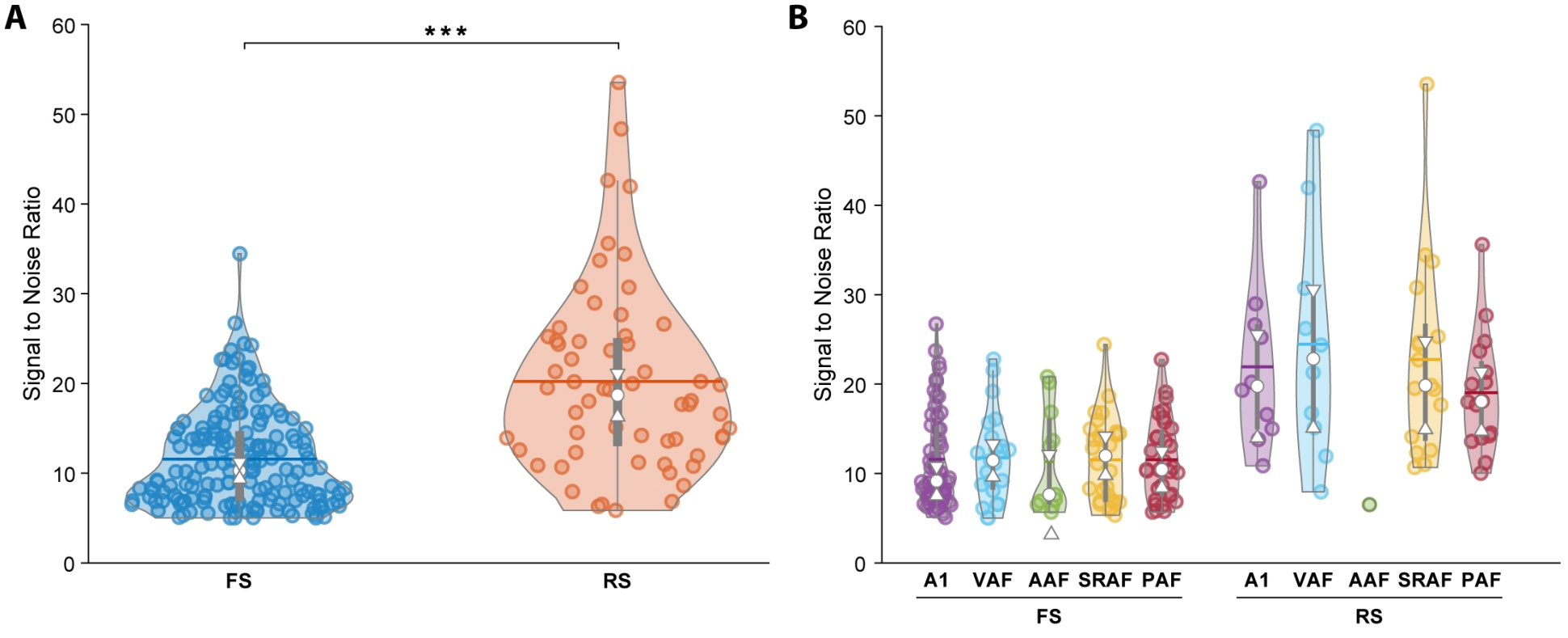
A
B
Signal to Noise Ratio
60
50
40
30
20
10
0
***
FS
RS
A1
VAF
AAF
SRAF
PAF
FS
RS